International Society for Rock Mechanics and Rock Engineering
Norwegian Group for Rock Mechanics
ISRM International Symposium
Eurock 2025 – Expanding the Underground Space
Trondheim, Norway, 16-20 June
ISBN 978-82-8208-079-8

Tension-torsion coupling effect and failure mechanism of anchoring section of anchor cable

Shuren Wang
School of Civil Engineering, Henan Polytechnic University, Jiaozuo, China
shurenwang@hpu.edu.cn *(email of corresponding author)*

Wenbing Guo
School of Energy Science and Engineering, Henan Polytechnic University, Jiaozuo, China

Abstract

For the anchor cable is a space spiral structure, there is reverse torque when it is pulled, and the existence of torque will reduce the axial tension and affect its anchoring performance. By using the self-developed cable tension-torsion coupling test system, three kinds of anchor cables with different diameters (9.5 mm, 12.7 mm, and 15.2 mm) commonly used in mining engineering were taken as the research materials, and the methods of indoor pull-out test, theoretical analysis and numerical simulation were adopted to study the coupling effect of tension and reverse torque of the anchor cable and the failure evolution process of the coupling force transfer of the anchor cable. Results show that the empirical formulas for calculating the torque of different diameters of anchor cables are fitted based on the torque-tension curve and the formula for calculating cable tension considering the decoupling of tension and reverse torque is presented based on the principle of work-energy. The expression of tension and torque of anchor cable is derived and the theoretical derivation is compared with the experimental results, and the accuracy of the mechanical model is verified. The equivalent stress, axial stress, shear stress and equivalent plastic strain of the section surface of the anchor cable under the condition of un- and free-rotation are analyzed by using numerical simulation. The tension-torsion coupling computational model of anchor cable is constructed to explain the failure evolution process of the anchoring system under the tension-torsion coupling effect. The axial tension and torque exhibit a cubic polynomial relationship in the first stage, which then transitions to a linear relationship as the conditions change. The results obtained can provide a solid foundation for tensile force analysis and anchorage force design of anchor cables.

Keywords

Anchor cable, Pull-out test, Tension-torsion coupling, Mechanical model, Failure mechanism

ISRM

NBG

1 Introduction

Anchor cable anchoring technology effectively controls deformation and enhances the stability of engineering rock and soil masses. This technology offers numerous advantages, including active support, security, and economy, making it widely applied in slope engineering, tunnel engineering, and mining engineering globally (Li et al. 2017; Li et al. 2022; Shi et al. 2024). While the rock bolt anchoring technology and anchor cable anchoring technology share similarities in the load transfer mechanism of the anchorage section, the pulling anchor cable produces a torque perpendicular to its section, causing the anchor cable strand to rotate reversely (Wang 2015). Pull-out tests indicate that if the anchor cable is allowed to rotate freely, each strand tends to slide along the original grooves of the anchoring resin, resulting in a torsional stress state. Conversely, if the anchor cable is constrained from rotating, the anchoring resin experiences both axial pull-out load and shear force when twisted, leading to complex stress states (Andrianov et al. 2020).

Over the years, several representative anchoring mechanical models have been developed for anchor cables, including the bond strength model, the axial force and torque model, and the shear model of structural planes. In the early 1990s, Kaiser et al. (1992) simplified the stranded cable structure into a polyline structure and proposed an anchoring mechanics model based on the radial displacement and lateral confining pressure of the structural plane. Considering the torque generated by the pull-out load of the anchor cable, Hyett et al. (1995) proposed a mechanical model of axial force and torque based on the modified Hoek anchorage unit. However, due to the torque being simplified as an equivalent axial force component, it was concluded that the torque generated by the axial pull-out load of the anchor cable was not in accordance with the actual situation, which was independent of the length of the anchorage segment. Since the 1970s, Farmer et al. (1975) proposed the elastic bond model of anchorage mechanics, which was theoretically deduced and experimentally verified to show that the axial force of the cable was attenuated exponentially along the axial direction.

In recent years, analytical expressions for the axial force of the anchor cable, the shear force of the structural plane, and the displacement of the anchorage element have been deduced by assuming the shear stress-strain curve of the structural plane as a three-stage line. This reflects the latest developments in current research (Li and Stillborg 1999; Cai and Champaigne 2012; Cao et al. 2014). Primarily, scholars in China have focused on the bond-slip constitutive relationship between steel reinforcement and concrete (Wang et al. 2017; Lin et al. 2019). Additionally, considering the heterogeneity and nonlinear failure properties of rock and soil masses, an analytic formula for load transfer in the anchorage segment has been deduced, and the coupling effect of the anchorage system has been verified (Zhang and Chen 2015; Li et al. 2021; Pytlik and Szot 2023). However, these studies primarily focus on the application of anchor cables and make simplifying assumptions in deriving theoretical formulas, largely ignoring the unwinding effect of torque generated during the pulling process of the anchor cable.

Since there are few reports on the failure of anchoring systems due to the torque decoupling effect in cable pulling tests, the understanding of the failure mode of the anchoring section and the constitutive relationship of the anchoring system needs further refinement. Based on the structural characteristics of anchor cables, this study enriches and develops the anchor cable anchoring theory by analyzing the coupling effect of anchor cable tension and torsional moment, as well as the failure mechanism of the anchoring section. This can provide a theoretical basis and technical support for engineering practice.

2 Materials and methods

2.1 Test materials and loading equipment

The test anchor cables, which were 1 × 7 steel strands produced by Tianjin Ruitong Limited Company, were made of high-carbon steel wire rod through cold drawing and twisting. These anchor cables came in three diameters (9.5 mm, 12.7 mm, 15.2 mm), and each diameter was available in three lengths (850 mm, 1150 mm, 1350 mm). These anchor cables were used in axial tensile experiments with locking lengths of 500 mm, 750 mm, and 1000 mm, respectively. The specification parameters of the anchor cables with different diameters are shown in Table 1.

Table 1 Main parameters of the anchor cables

Structure	Diameter (mm)	Cross-section area (mm^2)	Maximum load (kN)	Unit weight (kg/km)
1×7 Standard type	9.5	54.8	102	430
	12.7	98.7	184	775
	15.2	140	260	1101

The LW-1000 self-developed equipment was used for the test (Wang et al. 2020a), which comprises a loading device, a measuring device, and a data acquisition and processing system (Fig. 1). This equipment enables real-time data collection, instant display, and real-time chart plotting (1-Pedestal; 2-Cylinder body; 3-Lower beam; 4-Upper beam; 5-Piston rod; 6-Torque sensor; 7-Positioning pin; 8-Stretch rotating shaft; 9-Trolley track; 10-A car; 11-Anchor cable; 12-Concrete columns).

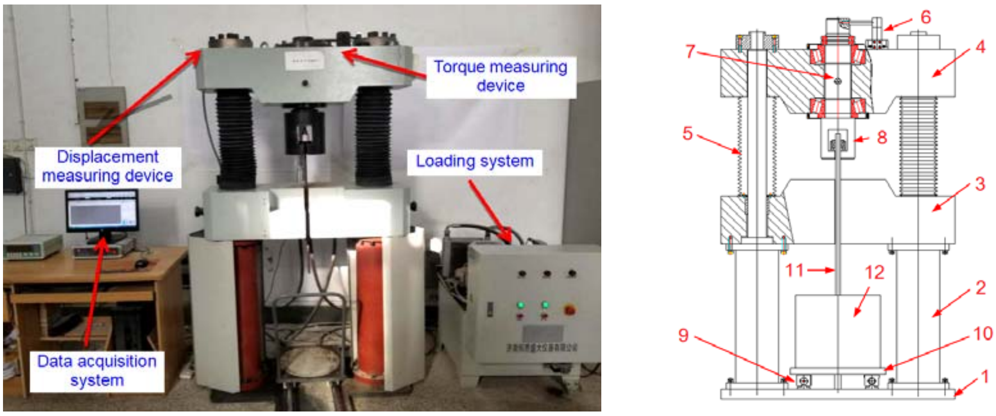

(a) Test equipment diagram (b) Structural diagram

Fig. 1 The loading and measurement device.

2.2 Computational model and calculation parameters

The three-dimension model of the steel strand was established by Abaqus (Wang et al. 2020b). The mesh division of the model is shown in Fig. 2. The material parameters of steel strand are measured according to the tensile test of steel wire. The constitutive parameters after transformation are shown in Table 2.

(a) Computational model (b) Cross-section of the model

Fig. 2 Computational model and its meshes of cable-bolts.

Table 2 Material parameters of steel strand.

Elastic modulus (GPa)	Poisson's ratio	Density (t/m^3)	Yield/Tensile strength (MPa)	Plastic train
210	0.30	7.85	1810/2020	0.05

2.3 Sample design and preparation

As shown in Figs. 3 and 4, the central pulling specimen was used in the test (Wang et al. 2020c; Wang et al. 2021). The anchor cable was anchored at the section center of the cylinder concrete specimen, and the anchorage segment was set at the middle and upper part of the central axis of the cylinder specimen. A total of 6 groups of specimens were made for the test, each group with 3 specimens. By changing confining pressure (0, 2.5, and 5.0 MPa) and the constraint conditions at the top of the anchor cable (non-rotation, free rotation), the influence rule of each factor change on the failure mode, ultimate bearing capacity and load-deformation curve of the internal anchorage segment were investigated.

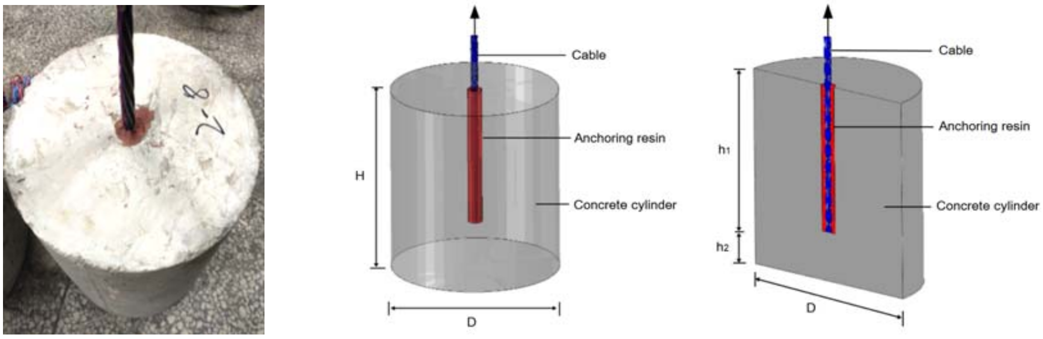

(a) Sample photo (b) Schematic diagram (c) Semi-cylindrical diagram

Fig. 3 Samples of pull-out test.

3 Results analysis and discussion

3.1 Characteristics analysis of Ten sion-displacement-torque curves

Since the locking length has little effect on the torque and tension, the typical axial force-displacement-torque curves of anchor cables with 12.7 mm anchor cable at a locking length of 500 mm are shown in Fig. 4(a). The displacement in Fig. 4 includes not only the tensile displacement of the steel strand, but also the sliding displacement between the steel strand and the clamp.

It can be found from Fig. 4(a), the axial force-displacement-torque curves of the anchor cables display three stages: Stage 1 (pre-tensioning stage), Stage 2 (elastic stage) and Stage 3 (plasticity stage). Based on the experimental data, the empirical formula for torque of anchor cable is fitted (R^2=0.99), and the torque expressions of anchor cables with different diameters are as follows:

$$M = cP\mathrm{d} = \left(0.025 + 7.045\times10^{-5} e^{0.318d}\right)Pd \tag{1}$$

Where M Torque of anchor cable, N·m;
P Axial force of anchor cable, kN;
c Torque coefficient;
d Anchor diameter, mm.

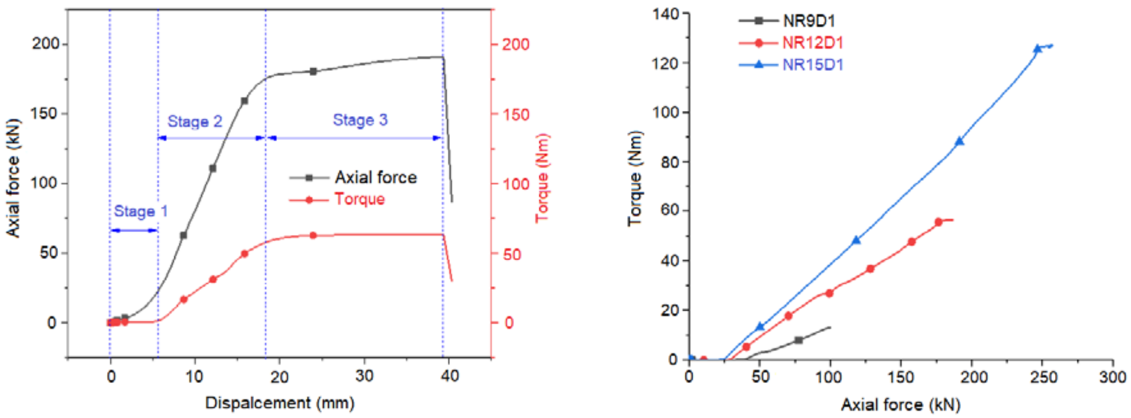

(a) 12.7 mm anchor cable (b) Axial force-torque curves

Fig. 4 Axial force-displacement-torque typicla curves and axial force-torque curves of different diameter cables.

3.2 Decoupling analysis of axial tensile force and torgue

Since the torque of the anchor cable is released under free rotation condition, part of the work done by pulling force is used to reverse, ignoring friction and other factors. The work induced by rotation of the anchor cable is equivalent to that of the reverse rotation force ΔF in tensile displacement. According to the work-energy principle:

$$W_1 - W_2 = \frac{\Delta FS}{2} \tag{2}$$

According to Eq. (2), the tension-torque coupling formula is proposed as follows:

$$\eta = \frac{\Delta F}{F} = \frac{2(W_1 - W_2)}{FS} \tag{3}$$

Where W_1 Work of the anchor cable performed under free rotation condition, J;
W_2 Work of the anchor cable performed under non-rotating condition, J;
ΔF Reverse rotation force, kN;
S Displacement, mm;
η Axial force-torque coupling coefficient.

Calculated according to the experimental data, the ratios of the tensile-torque coupling coefficients for the three diameters (9.5 mm, 12.7 mm, 15.2 mm) of the anchor cables are 11%, 12%, and 10%, respectively.

In general, the axial force-displacement curves obtained by the tests and numerical analysis match well, but the displacement of the elastic phase is not consistent. The main reason for this is that the experiment has a pretension stage, so there is nonlinear loading in the early stage, while the simulation is linear loading. However, the regularity of rotation and non-rotation remain the same, both stiffness decreases under free rotation condition.

3.3 Cross section stress analysis of anchor cable

3.3.1 Equivalent stress analysis of anchor cable

It is adopted the equivalent stress to analyze the comprehensive stress state of the anchor cable. Due to the stress distributions of the three kinds of the diameters are similar, the 15.2 mm cable was regarded as the example to analyze the tension-torsion coupling characteristics. When the strain in the elastic phase is 0.64%, the section equivalent stress distribution of the anchor cable under the conditions of restricted and free rotations are shown in Fig. 5.

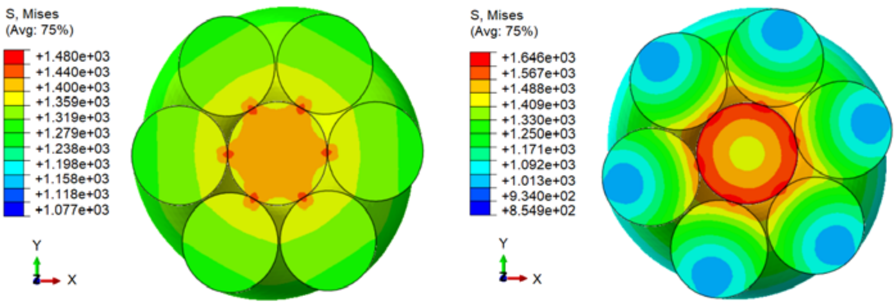

(a) Restricted rotation (b) Free rotation

Fig. 5 Equivalent stress of 15.2 mm diameter anchor cable under two conditions (MPa).

As seen from Fig. 5, in the case of the restricted rotation, the equivalent stress at the place where the internal and external steel wires contact is larger, followed by the central steel wire, and the outer steel wire of the anchor cable is the smallest. Due to the existence of the contact pressure, the local stress concentration occurs in the inner and outer contact areas, but it has little effect on the overall distribution. The stress distribution of the central steel wire is relatively uniform, and the outer steel wire decreases in layers from the inside to the outside of the anchor cable.Under the condition of the free rotation, it is also the place where the internal and external steel wires contact of the anchor cable is the largest, due to the influence of the torsion, there is a certain range of the stress concentration in the contact areas of the internal and external wires. Starting from the contact area, the central steel wire decreases from the outside to the inside in a concentric circle form, but the outer steel wire decreases from the inside to the outside in a half moon form, showing obvious delamination.

3.3.2 Axial stress analysis of tension-torsion coupling effects of anchor cable

When the strain is 0.64%, the axial stress of the cross-section of the anchor cable under the conditions of the restricted and free rotations is shown in Fig. 6. It can be seen from Fig. 6, the axial stress distribution of the anchor cable is relatively uniform without rotation, and the place where the inner and outer wires contact is smaller, because the place is not only pulled but also squeezed. Among these wires, the axial stress of the inner wire is the largest, and the outer wire decreases gradually from the inside to the outside, with a little change. Under the condition of the free rotation, the axial stress distribution is extremely uneven. The axial stress of the inner wire is larger, which of the outer wire is gradually reduced from the inside to the outside, the layering phenomenon is obvious.

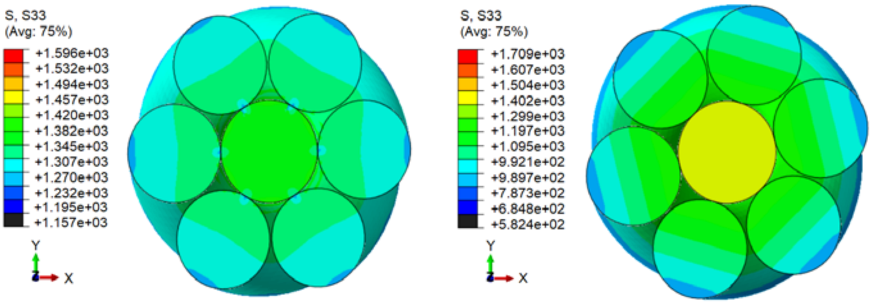

(a) Restricted rotation (b) Free rotation

Fig. 6 The cross-section axial stress under two conditions.

3.3.3 Shear stress analysis of tension-torsion coupling effects of anchor cable

As can be seen from Fig. 7, the shear stress of the inner wire under the restricted rotation condition is positive (untwisting direction) and approximately zero, indicating that it does not twist. The shear stress of the outer steel wire is negative (tight rotation direction), because it is restrained by the counter torque. In the case of the free rotation, the cross-section shear stress distribution is in a petal form, and the value of the contact area of the inner and outer wires is close and the direction is opposite, which indicates that the inner wire is also twisted by the shear effect of the outer wire, and the internal and external torque cancel each other. The central wire decreases in concentric circles from the outside to the inside, and the shear stress in the external wire gradually changes from negative to positive, and there is a critical layer in the middle of the anchor cable.

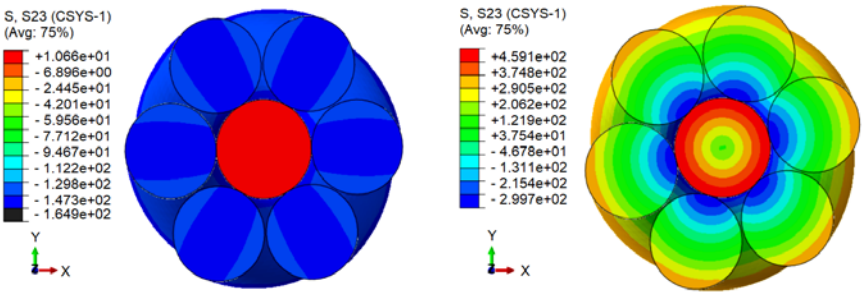

(a) Restricted rotation (b) Free rotation

Fig. 7 The cross-section shear stress under two conditions.

3.4 Constitutive relation of anchorage segment

As seen from Fig. 8(a), under the loading condition in the pull-out test, the free end of the anchor cable produces the torque perpendicular to its section. The load-torque-displacement curve consists of three characteristic stages, which can be divided into the loading stage, the softened stage, and the residual stage. Based on the experimental results, a theoretical model of the pull-out load-torque-displacement constitutive relationship before the residual failure was proposed.

The relation curve is named the YHW-FISH model, as shown in Fig. 8(b). The model can be divided into two stages: the loading stage and the softening stage. Since both the two stages are non-linear, the functional relationships of the YHW-FISH model can be expressed by Eqs. (3) and (4).

Loading stage:

$$\begin{aligned} F &= 171.07 - \frac{33572.75}{4(x-1.22)^2+196.56} \\ T &= -2.74\times10^{-3}x^3+0.26x^2-7.44x+11.36 \end{aligned} \qquad (0<x<x_1) \qquad (3)$$

Softening stage:

$$
\begin{aligned}
F &= 40.76+\frac{5891.25}{x}e^{-1.39\left[\ln\frac{x}{52.88}\right]^{2}} \\
T &= 1.26\times10^{-2}x^{2}+4.4x-205.85
\end{aligned}
\qquad (x_1 < x < x_2) \tag{4}
$$

Where F Pull-out load, kN;
T Torque, Nm;
x The corresponding slip, mm;
x_1 The dividing line between the loading stage and the softening stageorque, mm;
x_2 The dividing line of the softening stage and the residual stage, mm.

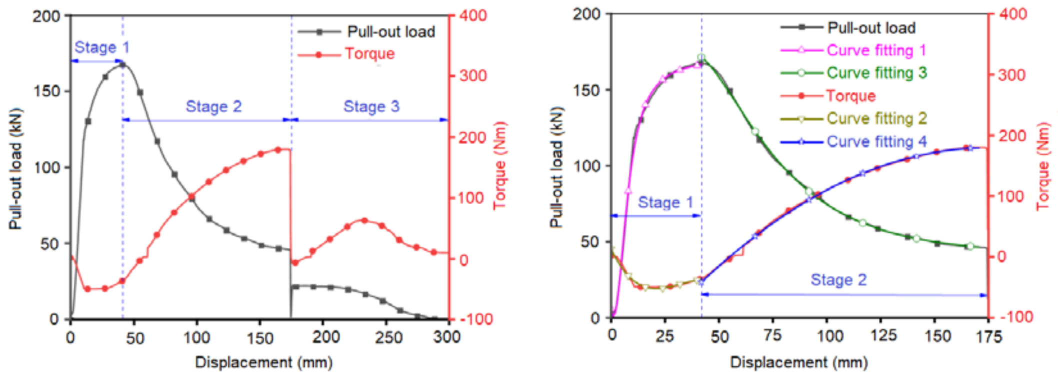

(a) The pull-out load-torque-displacement curves (b) The fitting curves

Fig. 8 The pull-out load-torque-displacement curves and the fitting curves.

Based on the above-mentioned analysis, the failure mechanism of the anchorage segment of the anchor cable can be obtained: the pull failure and shear failure are the main failure cause of the anchorage segment. But the pulling failure and the shear failure are not synchronous, the failure mechanism of the anchorage segment is the first pull and then shear. During the loading in the pull-out test, it mainly displays the pulling failure, and then the shear failure after pull-out load gradually reaching the peak value and which plays a leading role.

4 Conclusions

Based on the structural characteristics of the anchor cable, the coupling effect of tension and torsional moment, as well as the failure load mechanism of the anchor section, was analyzed through laboratory tests, numerical simulations, and theoretical analyses. The main conclusions obtained are as follows:

A formula for calculating cable tension, considering the decoupling of tension and inverse torque, is derived based on functional principles. The expressions for cable tension and torque are derived and experimentally verified. The maximum equivalent stress in the cable section occurs in the contact area between the inner and outer wires, and this stress is greater under free rotation than under restricted rotation.

The relationship between the torque of the anchor cable and the pulling load can be divided into two stages. In the loading stage, the torque increases with the increase of the pulling load until a peak value is reached, and then it decreases. The relationship between the pulling load and torque is described by a cubic polynomial. In the softening stage, the torque increases linearly as the pulling load decreases.

In this study, the load-torque-displacement coupling relationship of the anchor cable is established, providing a theoretical basis and technical support for engineering practice. Future research should focus on further studying the evaluation methods of load transfer characteristics and failure prediction methods for anchoring systems.

References

Andrianov IV, Danishevskyy VV, Topol H. (2020) Local stress distribution in composites for pulled-out fifibers with axially varying bonding. Acta Mechanica 231(5): 2065-2083. DOI: 10.1007/s00707-020-02634-6

Cai M, Champaigne D. (2012) Influence of bolt-grout bonding on MCB cone bolt performance. International Journal of Rock Mechanics and Mining Sciences 49: 165-175. DOI: 10.1016/j.ijrmms.2011.11.006

Cao C, Ren T, Cook C, Cao YJ. (2014) Analytical approach in optimising selection of rebar bolts in preventing rock bolting failure. International Journal of Rock Mechanics and Mining Sciences 72: 16-25. DOI: 10.1016/j.ijrmms.2014.04.026

Farmer IW. (1975) Stress distribution along a resin grouted rock anchor. International Journal of Rock Mechanics and Mining Sciences 12(11): 347-351. DOI: 10.1016/0148-9062(75)90168-0

Hyett AJ, Bawden WF, Macsporran GR, Moosavi M. (1995) Constitutive law for bond failure of fully-grouted cable bolts using a modified Hoek cell. International Journal of Rock Mechanics and Mining Sciences & Geomechanics Abstracts 32(1): 11. DOI: 10.1016/0148-9062(94)00018-X

Li C, Stillborg B. (1999) Analytical models for rock bolts. International Journal of Rock Mechanics and Mining Sciences 36(8): 1013-1029. DOI: 10.1016/S1365-1609(99)00064-7

Li DQ, Cai M, Masoumi H. (2021) A constitutive model for modified cable bolts exhibiting cone shaped failure mode. International Journal of Rock Mechanics and Mining Sciences 145: 104855. DOI: 10.1016/j.ijrmms.2021.104855

Li X, Si GY, Oh J, Corbett P, Xiang ZZ, Aziz N, Mirzaghorbanali A. (2022) Effect of pretension on the performance of cable bolts and its optimisation in underground coal mines with various geological conditions. International Journal of Rock Mechanics and Mining Sciences 152: 105076. DOI: 10.1016/j.ijrmms.2022.105076

Li XW, Aziz N, Mirzaghorbanali A, Nemcik J. (2017) Comparison of the shear test results of a cable bolt on three laboratory test apparatuses. Tunnelling and Underground Space Technology 61: 82-89. DOI: 10.1016/j.tust.2016.10.003

Lin HW, Zhao YX, Ozbolt J, Feng P, Jiang C, Eligehausen R. (2019) Analytical model for the bond stress-slip relationship of deformed bars in normal strength concrete. Construction and Building Materials 198: 570-586. DOI: 10.1016/j.conbuildmat.2018.11.258

Kaiser PK, Yazici S, Nosé J. (1992) Effect of stress change on the bond strength of fully grouted cables. International Journal of Rock Mechanics and Mining Sciences & Geomechanics Abstracts 29(3): 293-306. DOI: 10.1016/0148-9062(92)93662-4

Shi GC, Yang XJ, Sun JH, Tao ZG, Sousa LRE. (2024) Experimental study on the control characteristics of the negative Poisson's ratio structural anchor cable on the large deformation of rainfall-induced landslide. Bulletin of Engineering Geology and the Environment 83(4): 134. DOI: 10.1007/s10064-024-03641-w

Wang CH. (2015) Some end effects in a cylindrically orthotropic circular tube of finite length with radial inhomogeneity subjected to torsional loads. Acta Mechanica 226(6): 1707-1723. DOI: 10.1007/s00707-014-1283-1

Pytlik A, Szot M. (2023) Comparative testing of cable bolt and wire rope lacing resistance to static and dynamic loads. Archives of Mining Sciences 68(4): 707-724. DOI: 10.24425/ams.2023.148158

Wang Q, Wei ZZ, Xu G, Xiang J, Pan Q. (2017) Bond-slip model for reinforced concrete under deicer-frost environment. Journal of Building Materials 20(5): 692-699. DOI: 10.3969/j.issn.1007-9629.2017.05.006

Wang SR, Wang YH, Gong J, Wang ZL, Huang QX, Kong FL. (2020a) Failure mechanism and constitutive relation for an anchorage segment of an anchor cable under pull-out loading. Acta Mechanica 231(8): 3305-3317. DOI: 10.1007/s00707-020-02717-4

Wang SR, Wang YH, Wang ZL, Gong J, Li CL. (2021) Anchoring performances analysis of tension-torsion grouted anchor cable under free and non-free rotation conditions. DYNA 96(2): 166-172. DOI: https://doi.org/10.6036/9985

Wang SR, Wang ZL, Chen YB, Wang YH, Huang QX. (2020b) Mechanical performances analysis of tension-torsion coupling anchor cable. International Journal of Simulation Modelling, 19(2): 231-242. DOI: 10.2507/IJSIMM19-2-512

Wang SR, Wang ZL, Gong J, Wang YH, Huang QX. (2020c). Coupling effect analysis of tension and reverse torque during axial tensile test of anchor cable. DYNA, 95(3): 288-293. DOI: 10.6036/9603

Zhang X, Chen SH. (2015) Analytical solution for load transfer along anchored section of prestressed anchor cable. Rock and Soil Mechanics 36(6): 1667-1675. DOI: 10.16285/j.rsm.2015.06.019